DOI: 10.1007/s12541-012-0239-4

Optimal Design to Reduce the Maximum Load in Ring Rolling Process

Naksoo Kim[1], Honglae Kim[1], and Kai Jin[1,#]

1 Department of Mechanical Engineering, Sogang University, 35 Baekbeom-ro, Mapo-gu, Seoul, South Korea, 121-742
Corresponding Author / E-mail: jinkai@sogang.ac.kr, TEL: +82-2-705-8635, FAX: +82-2-712-0799

KEYWORDS: Ring rolling, Load minimization, Rolling schedule, Optimum design

Minimizing the maximum load on rolls in ring rolling process has been the most urgent demand in producing large rings made of high-strength material. With a view to meet the essential demand, the problem was solved by a novel process design, which respectively calculated the feed-rates of mandrel and axial rolls through optimum design. Based on the finite element simulation of ring rolling process by varying the feed-rates of the mandrel and axial rolls, an improved rolling schedule was established. The design of experiments via Taguchi method and the optimum design method such as Conjugate Gradient Method were used. The FE simulation was verified by comparison with experiment results. The optimized rolling schedule was suitable and reliable in the practical manufacture for both pure and radial-axial ring rolling process.

Manuscript received: December 2, 2011 / Accepted: May 22, 2012

NOMENCLATURE

$\bar{\sigma}$ = equivalent stress
$\dot{\bar{\varepsilon}}$ = equivalent strain rate
Ω = domain of the work-piece
S_f = forced boundary surface
τ_f = frictional stress
u_i = vector of nodal velocity
$\dot{\varepsilon}_v$ = volumetric strain rate
α = penalty constant
σ_{ij} = stress components
σ'_{ij} = deviatoric stress components
$\dot{\varepsilon}_{ij}$ = strain rate components
β = coefficient of angle
θ_A = angle of SMS node A
θ_B = angle of SMS node B
θ = angle of AMS node P
Δt = time increment
V_0 = initial volume of work-piece
V_1 = work-piece volume after updating AMS
$\bar{r}_1$ = mean ring radius after updating AMS
$\bar{r}_2$ = mean ring radius after corrected
$A(\theta)$ = ring cross-section area
Δr = correction value of radius
σ_f = flow stress
K_0 = stiffness coefficient
n = hardening coefficient
m = strain-rate sensitivity coefficient
F = feed force
R = electric resistance strain
A = conversion coefficient
η_1 = extreme ratio of the mandrel load
η_2 = extreme ratio of the axial roll load
i = designed case number
w_i = weighting factor
s = stroke of mandrel or axial roll
t = time variable.
$v_{f,\max}$ = maximum feed-rate of mandrel
$v_{a,\max}$ = maximum feed-rate of axial roll
v_{Rd} = linear velocity of driven roll
$v_{1,f}$ = variable of the mandrel feed speed
$v_{1,a}$ = variable of the axial roll feed speed
$MAX\,[L_{m,i}]$ = maximum mandrel load of simulation
$MAX\,[L_{a,i}]$ = maximum axial roll load of simulation
$MAX\,[L_{m,e}]$ = maximum mandrel load of experiment
$MAX\,[L_{a,e}]$ = maximum axial roll load of experiment
$(\dot{r},\dot{\theta},\dot{z})$ = velocity vector in cylindrical coordinate
(r,θ,z) = cylindrical coordinate

1. Introduction

Ring rolling is a process for creating seamless ring shaped components using specialized equipment and forming process. Rings are produced faster, more precisely and stronger than by this method those produced by other ring production methods. Rolled rings and related products have been used for many years in many applications such as bearings, ring gears and railroad wheels in the transportation industry; engine casings and engine disks in the aerospace industry; and tower connector flanges and electrical generator parts in the energy industry.[1]

The reduction of roller loads is a major challenge. If it is overcome, needless money and energy consumption will be saved by using low power ring rolling mills. Previously, many studies were conducted on the load of ring rolling process through experiment, theoretical analysis or numerical simulation. Johnson and Needham[2] attempted to calculate the load of the mandrel through fundamental analysis and experiment for the first time. Hawkyard et al.[3] employed a slip-line solution for indentation for determining the roll separating force. Thereafter, Ryoo and Yang[4] further demonstrated by applying the upper bound method to calculate the force of the driven roll and analyze the variable parameters which affected the load. In recent years, several attempts have been made in the analysis of the ring rolling process via the finite element method, abbreviated as FEM. The studies using FEM were extended from 2D to 3D, and analyzing by the rigid-plastic or elastic-plastic FE formulation. A complete 3D finite element method has been published by Huisman and Huetink.[5] Following which the full 3D ring rolling analysis was undertaken by Kim et al.[6] and subsequently Xu et al.[7] used 3D rigid-plastic FEM to calculate the load on the mandrel and the driven roll. Now, the study using FEM[8,9] has become a common method due to its predictability and accuracy.

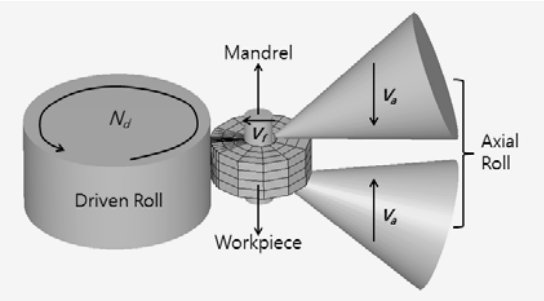

Fig. 1 Forming principle of radial-axial ring rolling

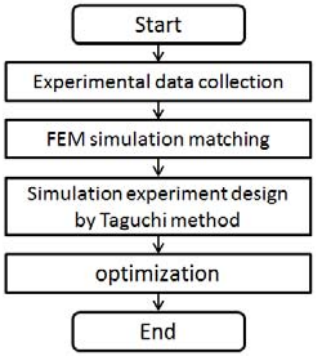

Fig. 2 Overall conceptual flowchart for the optimization schedule

However, most of these papers merely focused on the analysis of roller load by experiment or simulation without providing a useful method to reduce the load. Therefore, if there is a method that can be utilized to minimize the load especially the maximum load, it will reduce unnecessary expense and bring about huge economic benefit.

According to the analysis of Ryoo and Yang,[4] the main influencing factor of the load was the feed-rates of the mandrel and the axial rolls. Therefore, this paper focuses on filling the gap by providing a new feeding schedule via optimum design and FE simulation which employs commercial FEM software, SHAPE-RR. In order to verify this method, the concentration is on radial-axial ring rolling which was the most frequently used type in ring rolling process[10] as shown in Fig. 1. In this paper, the method combining experiment with simulation was employed for the development and verification of this feeding schedule. Finally, this optimization schedule as shown in Fig. 2 turned out to be an available and reasonable method in ring rolling process.

2. The finite element formulation

2.1 The rigid-plastic FEM

The rigid-plastic FEM is currently regarded as one of the most useful techniques for metal forming. The main advantage over other methods is that it enables the plastic deformation of complicated shapes to be simulated quite accurately. In this method, the elastic zone is neglected because the elastic deformation and elastic recovery after deformation are very small and typically negligible for bulk forming process. Thus, this method saves calculating time.[11]

Based on the variation principle of Markov-Hill,[12,13] the corresponding function of FEM solution in this method is briefly described for an arbitrary element of the work-piece as follows:

$$\Phi = \int_{\Omega} \bar{\sigma}\dot{\bar{\varepsilon}}\, dV - \int_{S_f} u_i \tau_f\, dS + \int_{\Omega} \frac{\alpha}{2} (\dot{\varepsilon}_V)^2\, dV \tag{1}$$

The inertial effects, body forces, and changes in geometry due to deformation are neglected. Then the velocity and stress fields satisfied the following conditions.

(i) Equilibrium equation

$$\sigma_{ij,j} = 0 \tag{2}$$

(ii) Flow-rule (constitutive equation)

$$\dot{\varepsilon}_{ij} = \frac{3}{2}\frac{\dot{\bar{\varepsilon}}}{\bar{\sigma}}\sigma'_{ij} \tag{3}$$

where $\bar{\sigma} = \left(\frac{3}{2}\sigma_{ij}\sigma_{ij}\right)^{\frac{1}{2}}$, and $\dot{\bar{\varepsilon}} = \left(\frac{2}{3}\dot{\varepsilon}_{ij}\dot{\varepsilon}_{ij}\right)^{\frac{1}{2}}$.

(iii) Relationship of strain rate-velocity (compatibility equation)

$$\dot{\varepsilon}_{ij} = \frac{1}{2}(u_{i,j} + u_{j,i}) \tag{4}$$

(iv) Incompressibility

$$\dot{\varepsilon}_V = 0 \tag{5}$$

The correct solution rendered the functional Φ to a minimum. Then, following the stationary-value principle, after differentiating Φ with respect to u_i, the equation was obtained in that the variables are the nodal velocities:

$$\frac{\partial \Phi}{\partial u_i} = 0 \tag{6}$$

The equation (6) was a non-linear equation taking the velocity components of the nodes as the unknown variables. The Newton-Raphson iteration method was employed to obtain the velocities.

2.2 Mesh system

Once the velocities were calculated according to the given geometry and the boundary conditions, the mesh system could be updated in accompaniment to its own shape changes. This numerical procedure is called updating of the mesh system.

Two kind of mesh systems were used for the simulation in ring rolling process. Spatial Mesh System (SMS) is a mesh system fixed in the space and Actual Mesh System (AMS) is a mesh system fixed to the work-piece. For the SMS, the fine mesh was applied only in main deforming region and others were rough mesh as presented in Fig. 3(a). It provided the velocity field to the AMS nodes and updated the AMS node velocities by linear interpolation, but the shape was updated according to that of the AMS node position by interpolation. For the AMS, it is a fine mesh system as presented in Fig. 3(b). All information of the work-piece (e.g., geometry of the work-piece, history of plastic deformation and effective stress etc.) was stored in AMS and calculated from node velocities that come from the SMS by linear interpolation. In this mesh method, velocity field was calculated and updated only in the SMS during the updating process. Thus, much time were saved compared to the traditional fine mesh method.

2.3 Algorithm of the finite element analysis

Usually, the algorithm of Rigid-plastic FEM is divided into two different procedures. One is to find the velocity field in the current configuration of work-piece and another is to update the geometry of the work-piece as the found velocities. The work-piece is represented numerically by the mesh system, which consists of nodes and elements. Combined Lagrangian-Eulerian method was used to update the configuration of the work-piece as seen in the flow chart shown in Fig. 4.

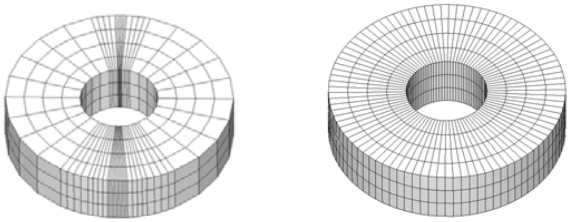

(a) SMS (Spatial Mesh System) (b) AMS (Actual Mesh System)

Fig. 3 Two types of mesh system

Actually, exact contact is impossible in FEM. Within a scheduled margin of error, rolls and work-piece are assumed to contact. The flow formulations suffered from volume loss. Meanwhile the volume growth of rings was a consequence of repeated projection of nodes along tangential velocities. To overcome both problems, cylindrical coordinate (r, θ, z) whose origin was at the center of the work-piece and whose z-axis was along the axis of the work-piece was employed. Kim et al.[6] proved that the volume kept constant by using angular velocity in the direction of rotation in interpolation. After determining the center of the work-piece, the velocity components of nodes changed from $(\dot{x}, \dot{y}, \dot{z})$ to $(\dot{r}, \dot{\theta}, \dot{z})$.

Under the CLE formulation, the SMS nodes were fixed in space. This meant that SMS nodes did not move in the circumferential direction nor coincide with the boundary of the material. Each increment proceeded as per the Lagrangian description by SMS and kept providing velocity field for the given geometry at time increments. Notably, the fixed angle position of the SMS nodes are generally in the same position as the free rotation of the ASM nodes. So, each node in the cylindrical system together with knowledge of the node numbering system was used to identify the AMS, and the velocities of the AMS node that moved with the material was obtained by linear interpolation from the SMS node velocities as illustrated in Fig. 5. For arbitrary AMS node P between SMS nodes A and B, the velocity field was expressed in the formula below:

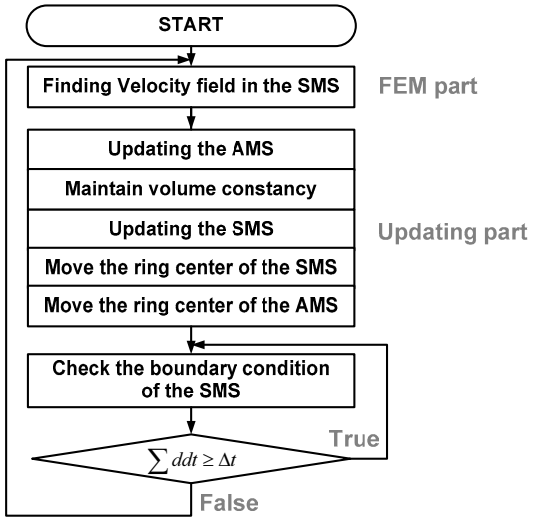

Fig. 4 Summary of Combined Lagrangian-Eulerian updating procedure

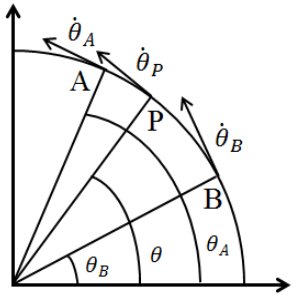

Fig. 5 Schematic diagram of the AMS node interpolation

$$\dot{r}_P = \dot{r}_A + \beta(\dot{r}_B - \dot{r}_A) \tag{7}$$

$$\dot{\theta}_P = \dot{\theta}_A + \beta(\dot{\theta}_B - \dot{\theta}_A) \tag{8}$$

$$\dot{z}_P = \dot{z}_A + \beta(\dot{z}_B - \dot{z}_A) \tag{9}$$

$$0 \le \beta = \frac{\theta_A - \theta}{\theta_A - \theta_B} \le 1 \tag{10}$$

Thus, the updated position of the AMS nodes could be calculated through the obtained velocities in the time increment Δt as follow equations (11-13). The displacement, strain, stress, etc. fields could also be obtained by the velocities. Repeating this process for all ASM nodes would give the updated mesh and other information.

$$r_P^{t+\Delta t} = r_P^t + \dot{r}_P \Delta t \tag{11}$$

$$\theta_P^{t+\Delta t} = \theta_P^t + \dot{\theta}_P \Delta t \tag{12}$$

$$z_P^{t+\Delta t} = z_P^t + \dot{z}_P \Delta t \tag{13}$$

After updating AMS nodes, the volume should remain unchanged. According to the method of K. Davey and M.J. Ward,[14] the angular and axial coordinates are considered as invariant and only the radial position is corrected. The correction value Δr of radius was based on the specific value between updated volume V_1 and initial volume V_0. The volume formulation related to radius was expressed:

$$V_1 = \int_0^{2\pi} \int_{A(q)} r dA dq = \overline{r}_1 \int_0^{2\pi} \int_{A(\theta)} dA d\theta \tag{14}$$

Then, the relation between volume and work-piece radius was obtained as follow:

$$\frac{V_1}{V_0} = \frac{\overline{r}_1}{\overline{r}_2} \tag{15}$$

The correction value Δr was imported by the definition:

$$\Delta r = \overline{r}_2 - \overline{r}_1 = \left(\frac{V_0}{V_1} - 1\right)\overline{r}_1 \tag{16}$$

For each AMS node, it added Δr in r-coordinate, so that the volume remained unchanged in the updating process.

The next step was to update the SMS nodes after correcting AMS nodes. Because the node coordinates of θ-direction in SMS were fixed, the nodes only changed in the r-direction and z-direction. The center of the work-piece was still unchanged and guaranteed the aspect ratio of elements during the updating stage, so the nodes in SMS were reconstructed based on AMS where geometry and material property were already updated in cylindrical coordinate system. Each node position of SMS was interpolated from both sides of the adjacent AMS nodes during the time increment Δt as shown in Fig. 6. After all SMS nodes were updated, the center of the work-piece would be recalculated and updated. Then, the process was repeated as the flow chat in the same increment Δt.

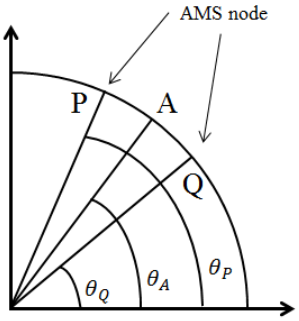

Fig. 6 Schematic diagram of the SMS node interpolation

3. Verification of the FEM software

In order to achieve the aim of the design, reliable FEM software was necessary. SHAPE-RR, which is a commercial simulation software using the mentioned finite element formulation was employed. However, the correctness of this software should first be verified. Thus, the verification test was carried out on the industrial-size ring rolling mill shown as Fig. 7 in Kaltek Co. Ltd. The feed speed of the test which was the feed speed of the practical production is shown in Fig. 8 and the work-piece material was AISI-304.

Table 1 AISI-304 material constants

Temp. (°C)	K_0 [MPa]	a_0	a_1	n	b_0	b_1	m
1100	160.00	0.00	2.14	0.09	0.00	0.10	0.10
1000	225.20	0.00	0.04	0.09	0.17	1.30	0.13
800	330.90	0.00	0.17	0.08	4.50	3.20	0.06

Fig. 7 The manufacture process in Kaltek Co. Ltd.

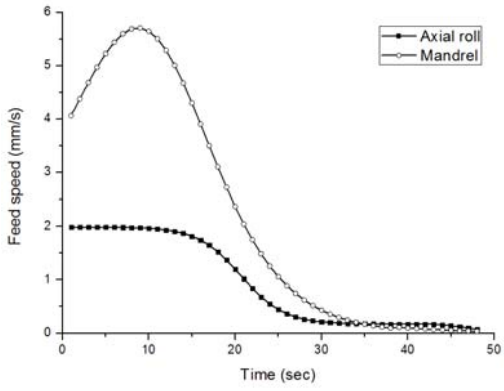

Fig. 8 The feed speeds in Kaltek Co. Ltd. experiment

The flow stress formula for the hot forming process is the following formula:

$$\sigma_f = K_0(a_0 + a_1\varepsilon)^n(b_0 + b_1\dot{\varepsilon})^m \tag{17}$$

The detailed material constants were checked and provided by Mongonon and Thomas,[15] shown in Table 1.

The working forces of mandrel and axial rolls were measured by the tool dynamometer, which was specially designed and manufactured to be the same as the measuring tool of Chul Kim etc..[16] It used the electric resistance strain gauge (EA-06-125BT-120, M-M Co.) and was calibrated in the calibration stand (Model B-2, LTV Aerospace Co.). The relation between the feed force and the electric resistance strain is as per the following equation:

$$F = AR \tag{18}$$

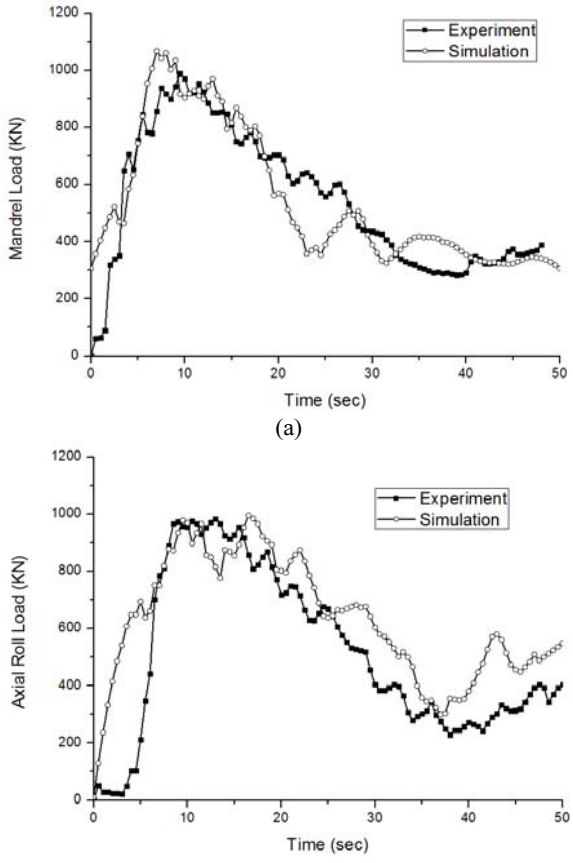

Fig. 9 Comparison of experiment and simulation

Table 2 Experimental condition for FE model verification

Parameters	Values
Initial outer diameter of the ring blank, D_0 (mm)	454
Initial inner diameter of the ring blank, d_0 (mm)	150
Initial height of the ring blank, h_0 (mm)	200
Expected outer diameter of the ring blank, D_1 (mm)	900
Expected inner diameter of the ring blank, d_1 (mm)	722
Expected height of the ring blank, h_1 (mm)	110
Radius of the driven roll, R_d (mm)	423
Radius of the mandrel, R_m (mm)	65
Radius of the axial roll, R_a (mm)	291
Length of the axial roll, L_a (mm)	800
Half of cone angle of the axial roll, φ (°)	20
Rotational speed of the driven roll, N_d (r/min)	40
Stroke of the mandrel, S_m (mm)	54
Stroke of the axial roll, S_a (mm)	32
Friction coefficient, μ	0.5
Temperature of environment, T_0 (°C)	20

In accordance with the experiment, all conditions were summarized in detail in Table 2. All rolls were assumed as the rigid body, and the initial ring blank was plastic in executing FE analysis.

The experiment and simulation results are illustrated in Fig. 9. Because of the influence of some uncertain factors such as friction change and temperature variation, some parts of the loads were non-coincidental, but the tendency of the curves was coincident. Thus, SHAPE-RR was confirmed to be reliable for the simulation of ring rolling process.

4. Optimal feed schedule

4.1 Maximum feed-rates of mandrel and axial roll

Before designing the ring rolling schedule, the constraints regarding the maximum feed-rates of mandrel and axial roll should be taken into account. Hua and Zhao[17] proposed the formulas for them as equations (19) and (21). The parameters were shown in Table 1.

$$v_{f,max} = \frac{2(\tan^{-1}\mu)^2 R_d^2 v_{Rd}}{\pi D_0\left(1+\frac{R_d}{R_m}\right)^2}\left(\frac{1}{R_d}+\frac{1}{R_m}+\frac{1}{R_0}-\frac{1}{r_0}\right) \tag{19}$$

$$v_{R1} = \frac{\pi N_d R_d}{30} \tag{20}$$

$$v_{a,max} = v_{f,max}\tan\varphi \tag{21}$$

$$\tan\varphi = \frac{h_0 - h_1}{(D_0 - d_0) - (D_1 - d_1)} \tag{22}$$

After calculation, the inequality constraints were obtained as follow:

$$0 \le v_f \le v_{f,\max} = 7.48 \text{ mm/s} \tag{23}$$

$$0 \le v_a \le v_{a,\max} = 4.43 \text{ mm/s} \tag{24}$$

4.2 Target function

The purpose of this paper is minimizing the maximum load. Therefore, a target function was needed to evaluate the optimized design. The extreme load ratio between the designed simulation case and Kaltek Co. Ltd. experiment was defined as the target function, illustrated as formula (25) and (26).

$$\eta_1 = \frac{MAX[L_{m,i}]}{MAX[L_{m,e}]} \tag{25}$$

$$\eta_2 = \frac{MAX[L_{a,i}]}{MAX[L_{a,e}]} \tag{26}$$

4.3 Trapezoidal feeding method

According to the analysis of Ryoo and Yang,[4] the main influencing factor of the load was the feed-rates of mandrel and axial roll. Therefore, a new trapezoidal feeding method shown in Fig. 10 was designed to achieve the goal for minimizing the maximum load. As a continuous feed method, the feed speed changed along the polygonal line as time passed. The area of the trapezoid was the total strokes of the process. Four variables were defined to describe the feed way and function. Therefore, the process was divided into 3 parts during the process time.

Consequently, if the strokes of mandrel and axial roll were represented as *s*, the relationship between stroke and feed-rate was established as equation (28) according to the area formula:

$$s = \frac{1}{2}t_1 v_1 + \frac{1}{2}(t_2 - t_1)(v_2 + v_1) + \frac{1}{2}(48 - t_2)v_2 \tag{27}$$

The strokes of mandrel s_m and axial roll s_a were respectively 54 mm and 32 mm in this process. Hence, the equation (27) was reduced to the following equations that were treated as equality constraints.

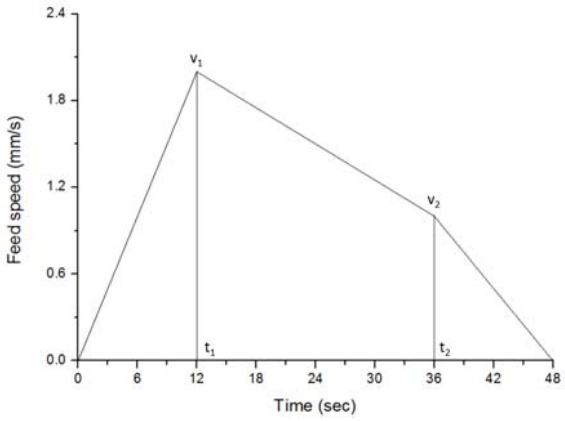

Fig. 10 Illustration of trapezoid feed method

Table 3 Orthogonal array and extreme value ratio

Case	No.	Time (t_1)	Time (t_2)	Feed speed (v_1)	Mandrel load ratio(η_1)	Axial roll load ratio(η_2)	Average ratio
1	1	6.0	30.0	1.0	0.775	0.944	0.860
	2	6.0	36.0	1.5	0.803	0.970	0.887
	3	6.0	42.0	2.0	0.753	0.935	0.844
	4	12.0	30.0	1.5	0.676	0.926	0.801
	5	12.0	36.0	2.0	0.713	0.913	0.813
	6	12.0	42.0	1.0	0.704	1,030	0.867
	7	18.0	30.0	2.0	0.669	0.923	0.796
	8	18.0	36.0	1.0	0.683	0.924	0.804
	9	18.0	42.0	1.5	0.638	0.969	0.804
2	1	6.0	30.0	0.6	0.925	0.856	0.891
	2	6.0	36.0	0.9	0.886	0.735	0.811
	3	6.0	42.0	1.2	0.817	0.891	0.854
	4	12.0	30.0	0.9	0.759	0.858	0.809
	5	12.0	36.0	1.2	0.776	0.798	0.787
	6	12.0	42.0	0.6	0.823	0.847	0.835
	7	18.0	30.0	1.2	0.770	0.887	0.829
	8	18.0	36.0	0.6	0.802	0.824	0.813
	9	18.0	42.0	0.9	0.881	0.844	0.863

For mandrel:

$$h_1 = \frac{1}{2}(t_2 v_1 - t_1 v_2 + 48 v_2) - 54 = 0\,[mm] \tag{28}$$

For axial roll:

$$h_2 = \frac{1}{2}(t_2 v_1 - t_1 v_2 + 48 v_2) - 32 = 0\,[mm] \tag{29}$$

Thereby, if we know any three variables, the other one could be derived. Hence, the total variables were reduced to three.

4.4 Taguchi orthogonal array

The experimental design proposed by the Taguchi method involved using orthogonal arrays to organize the parameters affecting the process and the levels at which they should be varied; it allowed for the collection of the necessary data to determine which factors affected product quality the most with a minimum amount of experimentation, thus saving time and resources.[18,19] The three variables of trapezoid feed method were specified with three levels for the ring rolling process. We arranged the experimental trials in an L9 (3^3) orthogonal array matrix.

In this process, two cases were designed. In case 1, the mandrel feed speed was set as trapezoid and the axial roll feed speed was still the same as the prior experiment before; In case 2, axial roll feed speed was set as trapezoid and the mandrel feed speed was still the same as the prior experiment. After calculation by equations (25)-(26), the target function results were shown in Table 3.

4.5 Optimization

So far, both speed for the mandrel and the axial rolls need to be optimized. Thus, it could be expressed as a multi-objective optimization problem. Furthermore, weighted sum method that is the most common approach was used like equation (30)

$$U = \sum_{i=1}^{k} w_i f_i \tag{30}$$

For easy comparison, we considered three optimal solutions for the rolling process. First, only mandrel was optimized (w_1=1, w_2=0); second, only axial rolls were optimized (w_1=0, w_2=1); third, combination was followed (w_1=0.5, w_2=0.5) since the sum of average ratio of case 1 was close to case 2. However, if variables (t_1, t_2, v_1) were changed, the variation of target function results remained unknown. Therefore, the approximation of the response function by Response Surface Method (RSM) was adopted to confirm it, which explored the relationships between explanatory variables and response variables.[20,21] Based on the Table 3, the object functions of mandrel and axial roll were obtained as follows:

$$f_1 = -0.126 - 0.015t_1 + 0.031t_2 + 0.556v_{1,f} + 0.235v_{1,f}^2 - 0.038t_2 v_{1,f} \tag{31}$$

$$f_2 = 5.082 + 0.005t_1 - 0.198t_2 + 0.002t_2^2 - 0.019t_2 v_{1.a} - 1.681v_{1.a} + 0.541v_{1.a}^2 \tag{32}$$

Therefore, this multi-objective optimization problem was expressed as follows:

$$\text{minimize} \quad U = w_1 f_1 + w_2 f_2$$

subject to

$$0 \le v_f \le v_{f,\max} = 7.48 \text{ mm/s}$$
$$0 \le v_a \le v_{a,\max} = 4.43 \text{ mm/s}$$

$$h_1 = \frac{1}{2}(t_2 v_{1,f} - t_1 v_{2,f} + 48 v_{2,f}) - 54 = 0$$
$$h_2 = \frac{1}{2}(t_2 v_{1,a} - t_1 v_{2,a} + 48 v_{2,a}) - 32 = 0 \quad (33)$$

To solve optimization problems, Conjugate Gradient Method (CGM) was used.[22,23] And the optimal results were shown in Table 4.

5. Results and discussion

Using optimal feed speeds of Table 4, the loads of mandrel and axial rolls were obtained as shown in Fig. 11. Thus, compared with the experiment results in the Kaltek Co. Ltd., the final reduction was listed in Table 5.

Results indicated that if we only optimized either mandrel or axial roll alternatively at the same time as other rolls were still kept intact, the loads were reduced more than the initial experiment results. And from Table 5 results, they were 17% and 23% reduction, respectively. It was put forth that if the mandrel and axial roll were considered and optimized at the same time, then both of them were reduced and can be seen easily in Fig. 11. The reductions of maximum value were 12% for mandrel and 17% for axial rolls. But in contrast, the degree of improvement was less than only considering one of them.

All maximum loads of optimal cases were smaller than the initial experiment. But mandrel and axial roll reductions were only 4% and 2% when only mandrel or axial roll was optimized. Thus, if only considering optimizing mandrel, there was not much influence for the maximum load of axial rolls seen from Fig. 11(a), or vice versa as shown in Fig. 11(b). But when compared with combination optimization, there was more influence on each other.

Compared with case results from the comparison curve Fig. 11, we discovered that the load curve of any roll became stable and reposeful if we optimized it. This meant the process of manufacture became stable and reposeful.

Table 4 Mandrel and axial optimal feed speed

Solution No.	t_1	t_2	$v_{1,f}$	$v_{1,a}$
1	18.0	42.0	2.0	-
2	10.0	36.0	-	1.0
3	20.0	36.0	1.7	1.2

Table 5 Optimal results of mandrel and axial roll

Case	Mandrel load ratio(η_1)	Axial roll load ratio(η_2)	Reduction of mandrel load	Reduction of axial roll load
1	0.83	0.96	17%	4%
2	0.98	0.77	2%	23%
3	0.88	0.83	12%	17%

6. Conclusions

The influence of process parameters on load has been analyzed and expressions for their influence have been formulated by using design method of optimum rolling schedule which minimized the maximum load on rolls.

(1) A range of feed rate which affected the loads of mandrel and axial roll has been proposed in Taguchi method results. The influence of the feed rate of mandrel and axial roll on the load has been explicitly evaluated and calculations have been compared with experimental results. This proposed feed rate of mandrel and axial roll was verified in theory by FE analysis.

(2) A newly developed method which was applied to minimize the maximum load exerted on rolls by establishing the rolling schedule has been proposed. The optimum design method was available in analyzing the interworking of the mandrel and the axial roll. As the variables are subdivided, better optimal results which satisfy the desire of designers are possible.

(3) When the proposed optimum rolling schedule is adapted to a real production process, the low power rolling mill can be used to produce the same size rings which could previously only be produced by large power mills. Thus, the manufacturers achieve more profits on the economic side in the ring rolling process.

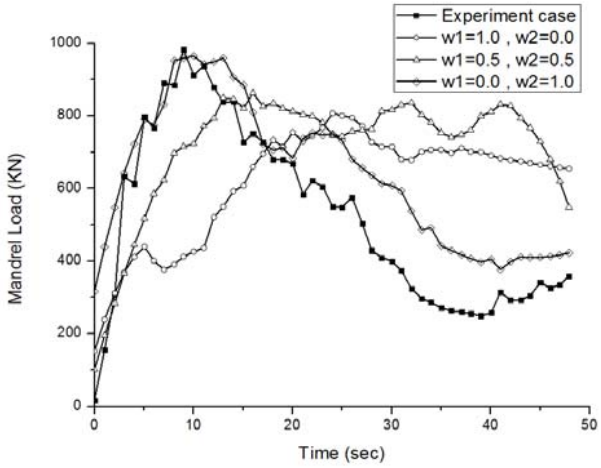

(a) Variation of load with time on mandrel

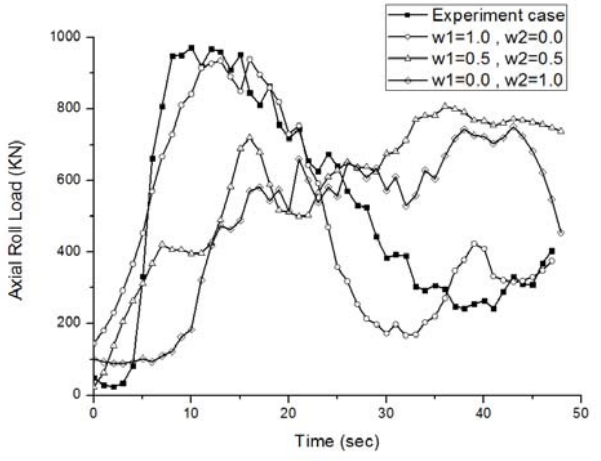

(b) Variation of load with time on axial roll

Fig. 11 Comparison of load

ACKNOWLEDGEMENTS

The study presented in this paper was supported by the Research Grant of Sogang University No. 201010042 and National Research Foundation of Korea No. 2012-0007756. The support is gratefully acknowledged.

REFERENCES

1. Bolin, R., "Ring Rolling in: Semiatin, S. L., ASM Handbook, Vol. 14 A Metalworking: Bulk forming," ASM Int., pp. 136-155, 2005.
2. Johnson, W. and Needham, G., "Experiments on ring rolling," Int. J. Mech. Sci., Vol. 10, No. 2, pp. 95-113, 1968.
3. Hawkyard, J. B., Johnson, W., Kirkland, J., and Appleton, E., "Analyses for roll force and torque in ring rolling, with some supporting experiments," Int. J. Mech. Sci., Vol. 15, No. 11, pp. 873-893, 1973.
4. Ryoo, J. S., Yang, D. Y., and Johnson, W., "The influence of process parameters on torque and load in ring rolling," J. Mech. Work. Technol., Vol. 12, No. 3, pp. 307-321, 1986.
5. Huisman, H. J. and Huetink, J., "A combined eulerian-lagrangian three-dimensional finite-element analysis of edge-rolling," J. Mech. Work. Technol., Vol. 11, No. 3, pp. 333-353, 1985.
6. Kim, N., Machida, S., and Kobayashi, S., "Ring rolling process simulation by the three dimensional finite element method," Int. J. Mach. Tool Manuf., Vol. 30, No. 4, pp. 569-577, 1990.
7. Xu, S. G., Lian, J. C., and Hawkyard, J. B., "Simulation of ring rolling using a rigid-plastic finite element model," Int. J. Mech. Sci., Vol. 33, No. 5, pp. 393-401, 1991.
8. Yea, Y., Ko, Y., Kim, N., and Lee, J., "Prediction of spread, pressure distribution and roll force in ring rolling process using rigid–plastic finite element method," J. Mater. Process. Technol., Vol. 140, No. 1-3, pp. 478-486, 2003.
9. Moon, H. K., Lee, M. C., and Joun, M. S., "Predicting polygonal-shaped defects during hot ring rolling using a rigid-viscoplastic finite element method," International Journal of Mechanical Sciences, Vol. 50, No. 2, pp. 306-314, 2008.
10. Guo, L. and Yang, H., "Towards a steady forming condition for radial–axial ring rolling," International Journal of Mechanical Sciences, Vol. 53, No. 4, pp. 286-299, 2011.
11. Kim, N., Kobayashi, S., and Altan, T., "Three-dimensional analysis and computer simulation of shape rolling by the finite and slab element method," Int. J. Mach. Tool Manuf., Vol. 31, No. 4, pp. 553-563, 1991.
12. Xu, Y., Zhang, S. H., Li, P., Yang, K., Shan, D. B., and Lu, Y., "3D rigid–plastic FEM numerical simulation on tube spinning," J. Mater. Process. Technol., Vol. 113, No. 1-3, pp. 710-713, 2001.
13. Guo, Y.-M., "A comparison between the rigid–plastic finite-boundary element method and the penalty rigid–plastic finite element method," J. Mater. Process. Technol., Vol. 101, No. 1-3, pp. 209-215, 2000.
14. Davey, K. and Ward, M. J., "A practical method for finite element ring rolling simulation using the ALE flow formulation," Int. J. Mech. Sci., Vol. 44, No. 1, pp. 165-190, 2002.
15. Mangonon, P. and Thomas, G., "Structure and properties of thermal-mechanically treated 304 stainless steel," Metall. Trans., Vol. 1, No. 6, pp. 1587-1594, 1970.
16. Kim, C., Jung, S. Y., and Choi, J. C., "A lower upper-bound solution for shear spinning of cones," Int. J. Mech. Sci., Vol. 45, No. 11, pp. 1893-1911, 2003.
17. Lin, H. and Zhi, Z. Z., "The extremum parameters in ring rolling," J. Mater. Process. Technol., Vol. 69, No. 1-3, pp. 273-276, 1997.
18. Peace, G. S., "Taguchi Methods: A Hands-On Approach," Addison-Wesley, pp. 114-128, 1993.
19. Chen, D.-C., You, C.-S., Nian, F.-L., and Guo, M.-W., "Using the Taguchi Method and Finite Element Method to Analyze a Robust New Design for Titanium Alloy Prick Hole Extrusion," Proc. Eng., Vol. 10, pp. 82-87, 2011.
20. Myers, R. H., Khuri, A. I., and Carter, W. H., "Response surface methodology: 1966-1988," Technometrics, Vol. 31, No. 2, pp. 137-153, 1989.
21. Castagliola, P., "Response Surfaces, Mixtures, and Ridge Analyses," J. of RSS (Series a-Statistics in Society), Vol. 171, No. 1, pp. 310-313, 2008.
22. Arora, J. S., "Introduction to optimum design, 2nd Ed.," Elsevier, pp. 296-299, 2004.
23. Davey, K. and Ward, M. J., "A successive preconditioned conjugate gradient method for the minimization of quadratic and nonlinear functions," Appl. Numer. Math., Vol. 35, No. 2, pp. 129-156, 2000.